Image Registration in Portable X-Ray Systems for Geometric Distortion Correction

Gavin Kelley
Electrical and Computer Engineering
University of North Carolina at Chalrotte
Charlotte, North Carolina
gkelley3@charlotte.edu

I. Introduction

A. Portable X-ray Systems

In hospitals, portable X-rays are typically administered to patients in the ICU or other units when they are too unstable to be transported to radiology. This practice avoids disrupting critical care (from intubation or IV drips) and reduces the infection risk from patient movement. Naturally, there are some trade-offs in image quality: portable chest X-rays are typically obtained in an Anterior-Posterior (AP) supine or semi-upright projection, rather than in the standard Posterior-Anterior (PA) upright view. The AP supine view is known to be more harmful and less informative than the PA view [1], with certain distortions, such as the heart appearing enlarged (it is farther from the detector, and the X-ray source is closer, resulting in greater beam divergence). Portable X-rays in the ICU are indispensable for continuous monitoring. They allow for the verification of medical device placement (such as endotracheal tubes and central lines) without moving the patient. Additionally, portable X-rays can be found in ambulances as well, for similar emergency medicine situations as in the ICU.

B. Geometric Distortions

Portable X-ray systems introduce geometric distortions due to non-ideal imaging geometry, limited patient positioning, and variable source-to-image distances (SID). In ICU or ambulance settings, the X-ray tube is often angled relative to the detector, producing perspective distortion where closer structures appear enlarged and parallel features converge. Even small angular deviations cause magnification and shape errors that can obscure diagnostic regions or complicate computer-aided analysis.

Distortion correction can be modeled as a geometric transformation between the captured and ideal image planes. An affine model accounts for translation, rotation, and shear, while a homography model (perspective transform) is required to handle more severe angle or depth variations. These transformations can be estimated through calibration phantoms or computational alignment methods.

Because few datasets include portable X-rays with known geometric offsets, synthetic distortions will be generated using existing chest radiograph databases. The specific dataset is described in Section III-A.

C. Image Registration and Mutual Information

Image registration involves aligning one image with a reference through transformations. In many cases of geometric distortion correction, registering a distorted image to an undistorted reference is typical. A powerful technique for automatic registration is to use mutual information (MI) as a similarity metric because it measures statistical dependence between image intensities and remains robust to differences in contrast and exposure.

In practice, using MI means defining a transformation, such as the affine or perspective transformation, with certain parameters, and then searching for the set of parameters that maximizes the MI between the transformed image and the reference. This search can be conducted via iterative optimization. In this work, the algorithm iteratively searches for affine parameters that maximize MI between a distorted X-ray and its reference, effectively realigning the image without explicit feature detection.

D. Project Objective

This project applies MI, a classical intensity-based registration method, to synthetic geometric distortions with the objective of evaluating the effectiveness of MI on these known distortions.

II. Related Work

MI is a classical registration metric that, despite the rise of learning-based approaches, remains widely used as a standard benchmark in contemporary research, such as in [2]. Originally introduced by Maes et al. in 1996 for multi-modality registration [3], MI established a robust statistical framework that continues to serve as a reference point for evaluating new methods.

For example, Wang and Chen (2013) proposed a hybrid elastic registration method for biological tissue and dental X-ray images that integrates both feature-based and area-based strategies [4]. In their study, MI is incorporated as part of the registration pipeline while also functioning as a comparative benchmark against which the effectiveness of their approach is measured.

III. Methodology

A. Dataset

As described in Section I-B, few datasets have an abundance of well-documented portable X-ray images with known geometric offsets, which makes it challenging to compare the registration results to a ground truth. The NIH Chest X-rays dataset will be used to distort fixed reference images to test the effectiveness of MI in registering X-ray scans with known geometric distortions. The evaluation will compare the recovered geometric parameters to the known ground truth and quantify the improvement in image alignment.

An advantage of this dataset is that several images are clearly marked as `portable`, which enables a realistic experiment for registering portable X-rays with real distortions.

B. Algorithm

SimpleElastix (SITK), an interface to the powerful image registration toolbox elastix, is built upon the core imaging library known as the Insight Segmentation and Registration Toolkit (ITK). It is an open-source framework capable of implementing this method and is chosen for its user-friendliness and Python integration. SITK has several built-in functions for both implementing distortion and registering the X-ray images. Several experiments will be designed to produce quantitative results to measure the effectiveness of MI registration.

The algorithm comprises three main stages:

- Pre-processing/Distortion
- Registration Procedure
- Post-Processing/Metric Evaluation

1) Pre-Processing and Distortion:

a) Image Loading and Pre-Processing: The algorithm first loads the fixed image, converts it to a single-channel format, and applies zero-padding to prevent boundary artifacts during geometric transformations. This ensures that subsequent distortions, such as rotation or shear, do not truncate the image content.

b) Synthetic Moving Image Generation: A synthetic moving image is generated by applying a composite geometric transformation to the padded fixed image. This transformation consists of a 2D Euler transform to introduce rotation and translation, followed by an affine transform to apply shear. The transformation parameters (rotation angle, translation, and shear factors) are defined as global variables and serve to simulate distortions commonly observed in portable X-ray acquisition. An example of a typical moving image after distortion is applied is shown in Fig. 1.

c) Noise Modeling: To approximate the quantum noise characteristics present in real X-ray systems, Poisson noise is added independently to both the fixed and moving images. The noise level is controlled through a scaling factor that adjusts the magnitude of the simulated photon-count variability. For all simulations performed, this noise factor is set to a modest value, as this is not the main focus of this work.

2) Registration Procedure:

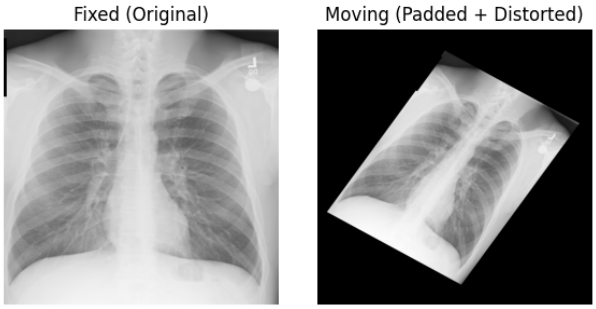

Fig. 1: Fixed vs. moving image example showcasing typical geometric distortions in this work

a) Composite Transform: Registration is performed using SITK's ElastixImageFilter in a two-stage framework. The first stage estimates a rigid transformation to correct for rotation and translation while preserving the size and shape of the image. The second stage performs an affine registration to capture the remaining geometric discrepancies, including shear. The SITK `CompositeTransform()` function enables these transformations to be implemented sequentially.

b) Parameter Tuning: In practice, these transformations are estimated using SITK parameter sets. SITK's `AdvancedMattesMutualInformation` is the built-in MI parameter, which is optimized to achieve better performance compared to the normalized version. The other SITK parameters of note are described as follows:

- **NumberOfSpatialSamples** specifies the number of sample points used from images to calculate the similarity metric.
- **MaximumNumberOfIterations** is the maximum number of optimization steps the algorithm will take to find the best transformation.
- **NumberOfResolutions** indicates that the registration will be performed in a multi-resolution (pyramid) fashion.

The number of computations that the algorithm performs is of the same order of magnitude as the product of these three parameters. Due to hardware restrictions and, therefore, long compile times, tuning these parameters required a simple but controlled experiment. In a separate spreadsheet, the accuracy of a known result was tracked as a function of run time, which is shown in Fig. 2. It was found that the registration accuracy remained constant when parameters were chosen so that the compile time did not fall below 13 seconds per image. The procedure for choosing these parameters was tedious and unintuitive; however, a reasonable compromise between performance and computation was determined. An example code snippet showcasing the parameter choice is shown in Fig. 3. This results in an average computation time of 13 seconds per image. For comparison, the point in Fig. 2 at 45 seconds per image used 12,000 spatial samples for the rigid registration and 15,000 for the affine registration (4,000 and 6,000 for 13 seconds, respectively). Additionally, the number of iterations was reduced from 400 to 200 and from 600 to

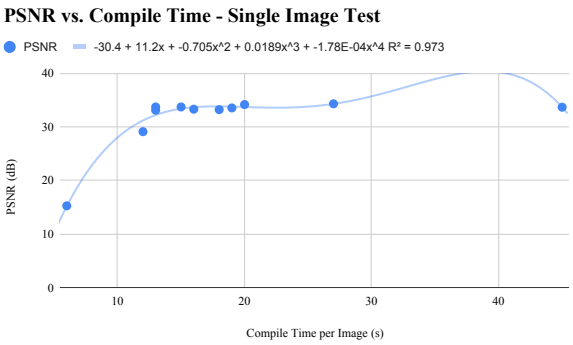

Fig. 2: Plot of PSNR vs. compile time for choosing registration parameters

```
pmap_rigid = sitk.GetDefaultParameterMap("rigid")
pmap_rigid["Metric"] =
     ["AdvancedMattesMutualInformation"]
pmap_rigid["NumberOfSpatialSamples"] = ["4000"]
pmap_rigid["MaximumNumberOfIterations"] = ["200"]
pmap_rigid["NumberOfResolutions"] = ["4"]

# (shortened here for brevity...)

pmap_affine = sitk.GetDefaultParameterMap("affine")
pmap_affine["Metric"] =
     ["AdvancedMattesMutualInformation"]
pmap_affine["NumberOfSpatialSamples"] = ["6000"]
pmap_affine["MaximumNumberOfIterations"] = ["450"]
pmap_affine["NumberOfResolutions"] = ["3"]
```

Fig. 3: Registration parameters, as shown in code

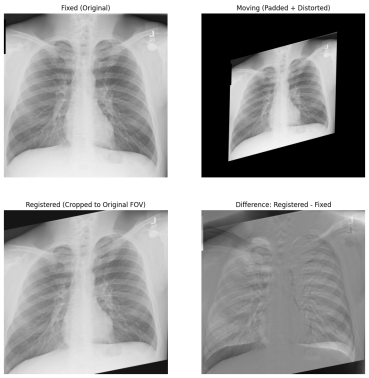

(a) Registration results for parameters resulting in 9 seconds per image

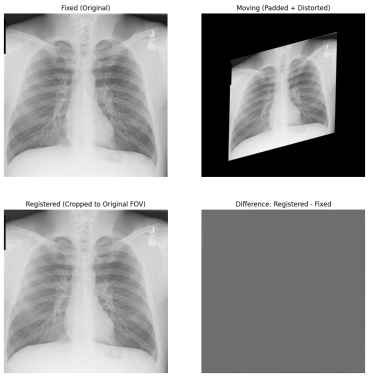

(b) Registration results for parameters resulting in 15 seconds per image

Fig. 4: Example simulation showcasing poor vs. desired registration results

450, respectively, achieving similar performance with more than a threefold reduction in computation time.

Finally, Figs. 4a and 4b showcase the difference between choosing parameters that result in 9 seconds per image and 15 seconds per image, respectively. The difference between these results is glaring, and emphasizes the importance of careful parameter tuning.

3) Post-Processing and Metric Evaluation: After registration, the aligned moving image is cropped back to the original spatial extent of the fixed image. Several quantitative metrics are then computed to evaluate registration quality, including Mean Squared Error (MSE), Peak Signal-to-Noise Ratio (PSNR), Normalized Cross-Correlation (NCC), and the Structural Similarity Index (SSIM). The algorithm returns these metrics in a pandas DataFrame format along with the final registered image.

C. Performance Metrics

As mentioned above, the MI registration is quantitatively evaluated by MSE, PSNR, NCC, and SSIM, which are all standard metrics in the image registration literature. They are briefly defined and described in this section.

1) Mean Squared Error: MSE is defined as

$$\mathrm{MSE} = \frac{1}{mn} \sum_{i=0}^{m-1} \sum_{j=0}^{n-1} [I(i,j) - K(i,j)]^2 \tag{1}$$

where I is an $m \times n$ image and K is an approximation of this image. In this work, I refers to the fixed image and K is the synthetically-distorted moving image.

2) Peak Signal-to-Noise Ratio: The PSNR (in dB) is defined using (1) as

$$\mathrm{PSNR} = 10 \log_{10} \left(\frac{\mathrm{MAX}_I^2}{\mathrm{MSE}} \right) \tag{2}$$

where MAX_I is the maximum possible pixel value of the image.

3) Normalized Cross-Correlation: The NCC between the same two $m \times n$ images I and K as in (1) is defined as

$$\mathrm{NCC} = \frac{1}{\sigma_I \sigma_K} \sum_{m,n} \left[I - \overline{I} \right] \left[K - \overline{K} \right] \tag{3}$$

where $\overline{I}$ and $\overline{K}$ are the mean intensity values, and σ_I and σ_K are the standard deviations of I and K, respectively.

4) Structural Similarity Index: The SSIM is defined as

$$\mathrm{SSIM}(x,y) = \frac{(2\mu_x\mu_y + C_1)(2\sigma_{xy} + C_2)}{(\mu_x^2 + \mu_y^2 + C_1)(\sigma_x^2 + \sigma_y^2 + C_2)} \quad (4)$$

where Table I briefly summarizes the parameters in (4).

TABLE I: Summary of SSIM statistical parameters

Parameter	Description
μ_x	Sample mean of image x
μ_y	Sample mean of image y
σ_x	Sample variance of image x
σ_y	Sample variance of image y
σ_{xy}	Sample covariance between x and y
C_1, C_2	Stabilizing constants to avoid division by small denominators

IV. Results and Analysis

This section presents the quantitative results for determining the effectiveness of MI registration. First, a representative simulation is performed to analyze the distribution of registration metrics. Then, two experiments are conducted to investigate the transformation parameters at which MI registration is no longer reliable, which describe the bounds within which MI can be considered accurate and clinically useful for portable X-ray alignment.

A. Representative 25-Image Simulation

A representative sample of the dataset was selected from 25 X-ray images, including three portable X-ray scans. For this simulation's moving image distortion, the rotation angle was set to $\theta = 30°$ (large rotation), the translation parameters were set to $t_x = 5.0$, $t_y = -10.0$ (small translation), and the shear factors were set to $k_x = 0.2$, $k_y = 0.1$ (modest shear). The quantitative results for this 25-image simulation are characterized by Figs. 5 and 6, which show the registration metric distributions and PSNR vs. SSIM, respectively. These

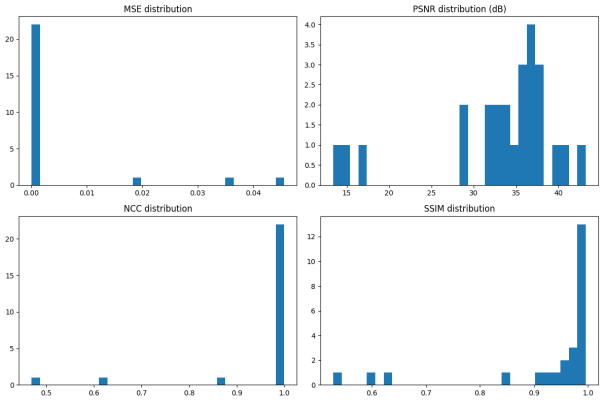

Fig. 5: Distributions of Registration Metrics for 25-image simulation

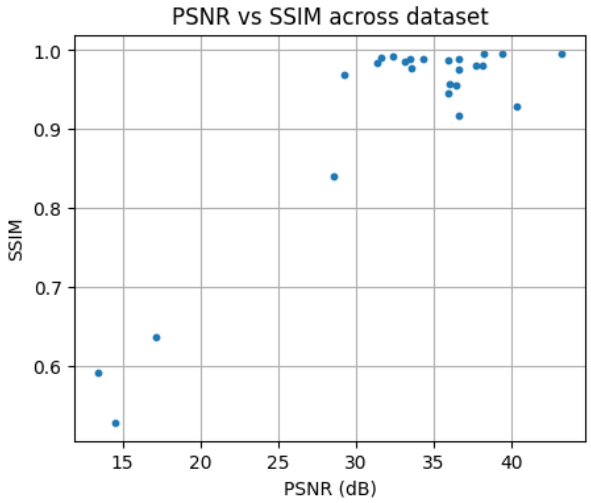

Fig. 6: PSNR (dB) vs. SSIM for 25-image simulation

plots clearly show that the MSE is low, while the PSNR, NCC, and SSIM values are sufficiently high for a majority of the scans. A summary of the quantitative results can be seen in Table II, where the 4th, 5th, and 6th rows of data indicate the percentiles of the sample.

TABLE II: Summary of metrics for 25-image simulation

	MSE	PSNR	NCC	SSIM
mean	4.35E-03	32.954	0.958	0.923
std	1.16E-02	7.552	0.129	0.133
min	4.76E-05	13.410	0.469	0.528
25%	2.17E-04	31.612	0.998	0.946
50%	2.54E-04	35.958	0.9996	0.981
75%	6.90E-04	36.642	0.9998	0.989
max	4.56E-02	43.226	0.9998	0.996

B. Experiment 1: Metrics vs. Rotation Angle

To evaluate the robustness of the registration algorithm to rotational misalignment, a controlled rotation-sweep experiment was conducted. In the control condition, all other geometric transformation parameters were set to zero, and the rotation angle of the moving image was varied from - 30° to 30° in uniform increments. For each rotation level, registration was performed on five randomly selected images drawn from the previously defined set of 25 representative chest X-rays. The resulting performance curves in Fig. 7 demonstrated that the algorithm maintained consistently high registration quality—across all four metrics (MSE, PSNR, NCC, and SSIM)—throughout a broad interval from approximately - 10° to 20°. Within this range, the metrics were both stable and near their optimal values.

A second experiment introduced a more realistic distortion scenario to simulate conditions commonly observed in

portable X-ray acquisition. In this simulation, the same rotation sweep from - 30° to 30° was performed, but with modest geometric distortions applied: horizontal and vertical translations of $t_x = 5.0$ and $t_y = -10.0$, as well as shear factors $k_x = 0.2$ and $k_y = 0.1$. Under these conditions, the region of stable high-quality performance narrowed significantly, as shown in Fig. 8. Metrics remained both strong and relatively constant only within a restricted interval of roughly - 5° to 10°, indicating increased sensitivity to rotation when compounded with translation and shear distortions. As expected, the average values of MSE, PSNR, NCC, and SSIM were all lower relative to the control case, reflecting the additional difficulty introduced by simultaneous distortions a summary of the MI performance is outlined in Table III.

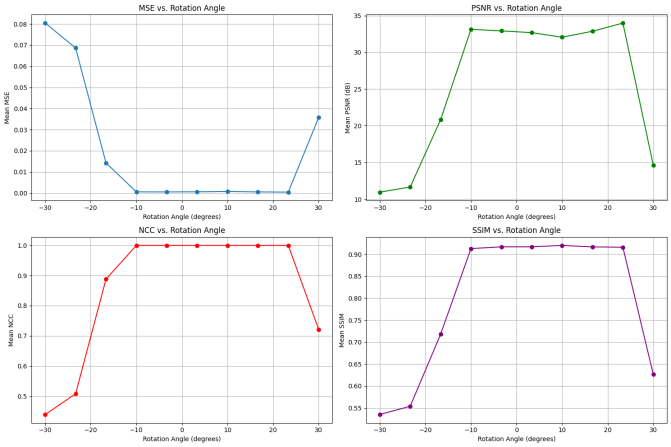

Fig. 7: Registration metrics vs. rotation angle θ, control

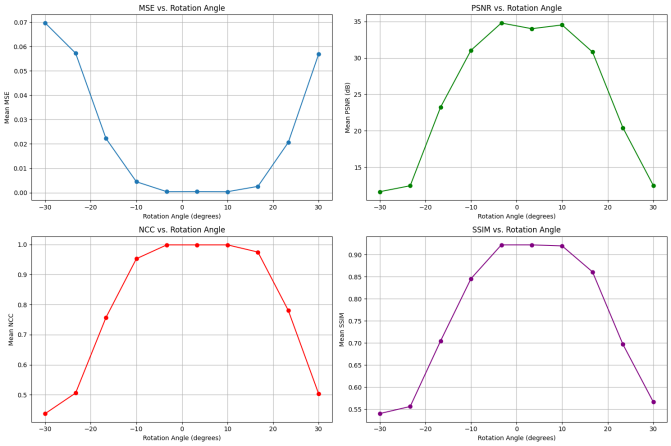

Fig. 8: Registration metrics vs. rotation angle θ, distorted

C. Experiment 2: Metrics vs. Shear Factors

To investigate the effect of shear distortions on registration performance, two independent parameter sweeps were conducted: one varying the horizontal shear factor k_x and another varying the vertical shear factor k_y. In both cases, the shear parameter was incremented from 0.0 to 0.3, while all other

TABLE III: Summary of metrics vs. rotation angle distortion

Control Moving Image				
	MSE	**PSNR**	**NCC**	**SSIM**
mean	0.020262	25.574718	0.855335	0.793313
std	0.029932	9.819792	0.214739	0.168459
min	0.000227	10.665315	0.402141	0.457625
25%	0.000451	14.497279	0.738525	0.638389
50%	0.000817	30.970399	0.999009	0.908687
75%	0.035522	33.459819	0.99931	0.920565
max	0.085796	36.432847	0.999364	0.927183
Distorted Moving Image				
	MSE	**PSNR**	**NCC**	**SSIM**
mean	0.023493	24.545721	0.790735	0.753424
std	0.028052	10.738765	0.245956	0.182543
min	0.000166	10.961812	0.340247	0.487374
25%	0.000322	13.087291	0.540999	0.556184
50%	0.000857	30.697936	0.99773	0.907901
75%	0.049121	34.918048	0.998911	0.915393
max	0.080134	37.803973	0.99933	0.935059

transformation parameters were initially set to zero to form a control condition. As with the rotation experiment, each shear level was evaluated using five randomly selected chest X-rays from the representative set of 25 images. Across both k_x and k_y control simulations, the metrics exhibited some fluctuations from point to point, resulting in slightly jagged performance curves, as shown in Figs. 9 and 10. However, the absolute differences across each sweep remained small, and all four metrics (MSE, PSNR, NCC, SSIM) stayed within a narrow, high-performing range. This behavior indicates that under isolated shear distortions (without the presence of rotation or translation), the registration algorithm remains stable and relatively insensitive to modest shear variations.

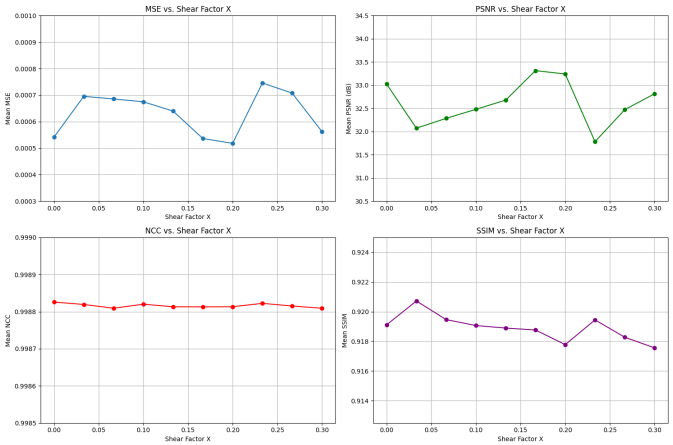

Fig. 9: Registration metrics vs. Shear Factor k_x, control

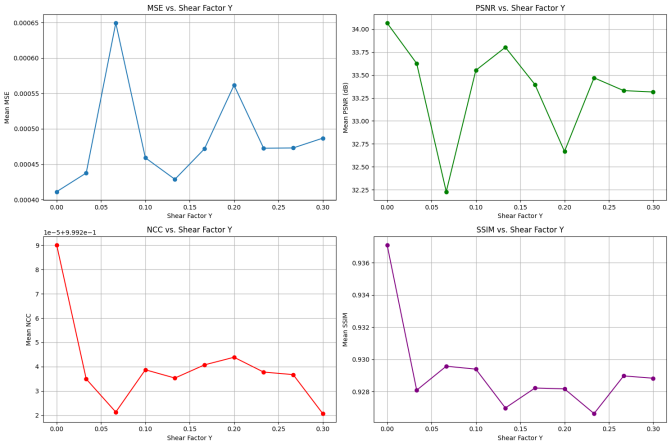

Fig. 10: Registration metrics vs. Shear Factor k_y, control

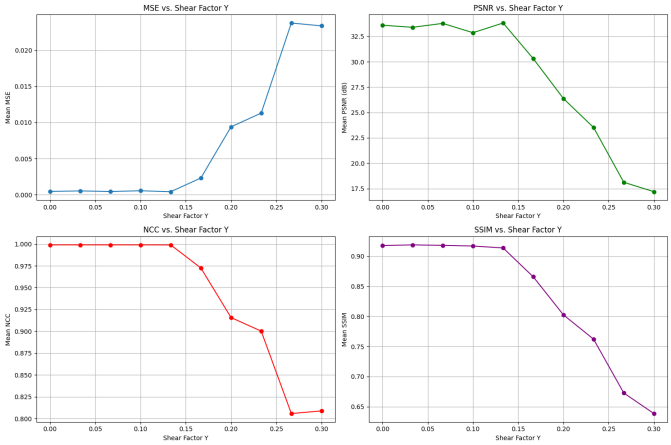

Fig. 12: Registration metrics vs. Shear Factor k_y, distorted

A second set of simulations introduced combined geometric distortions to emulate more realistic portable X-ray conditions, similar to those of the rotation angle experiment. For both the k_x and k_y sweeps, the following baseline distortions were applied prior to registration: a rotation of $\theta = 10°$, translations of $t_x = 5.0$ and $t_y = -10.0$, and the complementary shear component fixed to the values used in the previous rotation experiment. Specifically, for the k_x sweep, k_y was set to 0.1, while for the k_y sweep, k_x was fixed at 0.2. Under these distortion conditions, the algorithm's performance remained strong over the first portion of each shear sweep, but a clear breakdown was observed beyond a critical threshold. For the k_x simulation, all metrics remained robust up to approximately $k_x = 0.25$, after which a pronounced roll-off occurred at the final point $k_x = 0.3$ (Fig. 11). A similar trend appeared in the k_y results, though with a notably lower tolerance: the onset of significant degradation occurred at roughly $k_y = 0.15$ (Fig. 12). This comparative behavior suggests that the MI registration is more sensitive to vertical shear than horizontal shear when combined with rotation and translation distortions.

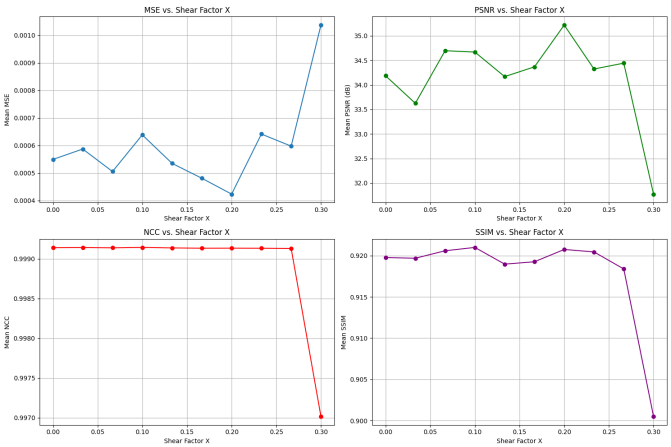

Fig. 11: Registration metrics vs. Shear Factor k_x, distorted

Finally, the quantitative results for the horizontal and vertical shear simulations are displayed in Tables IV and V, respectively. For the k_x simulation, the mean metric values between the control and distorted cases are nearly identical, which is expected given that only a single shear level exhibited a substantial drop in performance. In contrast, the k_y simulation shows noticeably lower averages across all metrics, reflecting the earlier onset of performance degradation observed in the vertical shear sweep. These findings complete the assessment of geometric sensitivity and establish a foundation for determining acceptable distortion limits in downstream analyses.

TABLE IV: Summary of metrics vs. horizontal shear distortion

	Control Moving Image			
	MSE	**PSNR**	**NCC**	**SSIM**
mean	0.000631	32.615742	0.998816	0.918909
std	0.000319	2.477735	0.000499	0.007305
min	0.000159	28.086319	0.997894	0.906389
25%	0.000428	31.181275	0.998754	0.912779
50%	0.000600	32.215733	0.998940	0.916519
75%	0.000762	33.686469	0.999179	0.924334
max	0.001554	37.986211	0.999331	0.931531
	Distorted Moving Image			
	MSE	**PSNR**	**NCC**	**SSIM**
mean	0.000600	34.147477	0.998925	0.917933
std	0.000608	4.030808	0.001497	0.016905
min	0.000107	26.539721	0.988644	0.825702
25%	0.000178	31.271536	0.999171	0.914762
50%	0.000302	35.205183	0.999239	0.921802
75%	0.000746	37.494076	0.999259	0.929715
max	0.002218	39.722544	0.999276	0.932801

TABLE V: Summary of metrics vs. vertical shear distortion

	MSE	PSNR	NCC	SSIM
Control Moving Image				
mean	0.000485	33.345816	0.999240	0.929201
std	0.000159	1.327016	0.000118	0.007870
min	0.000248	29.616967	0.999032	0.913017
25%	0.000362	32.261283	0.999160	0.924586
50%	0.000455	33.422642	0.999295	0.927914
75%	0.000594	34.411475	0.999320	0.935884
max	0.001092	36.063128	0.999433	0.947644
Distorted Moving Image				
	MSE	**PSNR**	**NCC**	**SSIM**
mean	0.007260	28.296524	0.939770	0.832760
std	0.012111	7.676688	0.110235	0.129959
min	0.000231	14.003109	0.582180	0.584239
25%	0.000433	20.461290	0.944991	0.681504
50%	0.000570	32.440065	0.999252	0.909485
75%	0.009022	33.633656	0.999291	0.914586
max	0.039782	36.369740	0.999397	0.932664

V. Conclusions

This work evaluated the sensitivity of MI–based image registration to a variety of geometric distortions representative of those encountered in portable chest X-ray radiographs. Across all experiments, including isolated and combined rotations, translations, and shear transformations, the MI algorithm demonstrated strong robustness over a wide operational range. In the control simulations, performance remained consistently high even as individual distortion parameters were swept across clinically realistic intervals. When multiple distortions were introduced simultaneously, the algorithm continued to register images effectively, with degradation occurring only beyond well-defined thresholds. Notably, the method exhibited greater sensitivity to vertical shear and compounded distortions, but still maintained acceptable accuracy within the ranges most commonly produced during bedside imaging.

These findings address the suitability of mutual information as a benchmark metric for portable X-ray registration. Portable radiography is inherently prone to misalignment due to patient positioning constraints, variable source–detector geometry, and limited technologist control in emergency or ICU environments. The demonstrated robustness of MI across diverse distortion conditions indicates that it can reliably accommodate the geometric variability typical of these settings. As a result, MI-based registration provides a strong foundation for downstream tasks. Ultimately, this work establishes quantitative performance boundaries that can guide the development and evaluation of registration pipelines intended for real-world portable X-ray applications.

References

[1] F. Ata, P. Iqbal, B. Muthanna, and Z. Anwer, *"Use of AP Vs PA view chest X rays in Medical facility of Hamad General Hospital Doha, Qatar."*, 10 2018.

[2] Y. Huang, A. Maier, F. Fan, B. Kreher, X. Huang, R. Fietkau, C. Bert, and F. Putz, "Learning perspective deformation in x-ray transmission imaging," 2023.

[3] F. Maes, A. Collignon, D. Vandermeulen, G. Marchal, and P. Suetens, "Multi-modality image registration by maximization of mutualinformation," vol. 16, pp. 14–22, 07 1996.

[4] C.-W. Wang and H.-C. Chen, "Improved image alignment method in application to x-ray images and biological images," *Bioinformatics*, vol. 29, pp. 1879–1887, 05 2013.